PHYSICAL REVIEW B VOLUME 62, NUMBER 22 1 DECEMBER 2000-II

Dynamical phases of driven vortices interacting with periodic pinning

Gilson Carneiro*
Instituto de Física, Universidade Federal do Rio de Janeiro, Caixa Postal 68528, 21945-970, Rio de Janeiro-RJ, Brazil
(Received 15 September 2000)

The finite temperature dynamical phases of vortices in films driven by a uniform force and interacting with the periodic pinning potential of a square lattice of columnar defects are investigated by Langevin dynamics simulations of a London model. Vortices driven along the [0,1] direction and at densities for which there are more vortices than columnar defects ($B>B_\phi$) are considered. At low temperatures, two dynamical phases, elastic flow and plastic flow, and a sharp transition between them are identified and characterized according to the behavior of the vortex spatial order, velocity distribution, and frequency-dependent velocity correlations.

There is a great deal of current interest in the study of dynamical phases of vortices driven by an external force and interacting with various arrays of pinning centers. One possibility is periodic pinning resulting from a lattice of artificial defects. Understanding the dynamical phases in this case is of interest because it may be possible to observe them in superconducting films with periodic arrays of holes, magnetic dots and columnar defects (CD). Several techniques have been developed to fabricate these films and studies of vortex dynamics in them have been reported.[1,2] Theoretical workers have carried out investigations, mostly numerical, of driven vortices under periodic pinning.[3–6] However, as discussed here, several questions remain open.

To be specific, this paper considers two-dimensional vortices interacting with a columnar defect lattice (CDL). The motion of N_v such vortices is assumed to be governed by Langevin equations for massless particles, which for the lth vortex reads,[7]

$$\eta\frac{d\mathbf{r}_l}{dt}=\mathbf{F}_l^{vv}+\mathbf{F}_l^{v-cd}+\mathbf{F}_d+\mathbf{\Gamma}_l, \tag{1}$$

where η is the friction coefficient, $\mathbf{F}_l^{vv}=-\Sigma_{j\neq l=1}^{N_v}\nabla_l U^{vv}(\mathbf{r}_l-\mathbf{r}_j)$ is the force of interaction with other vortices, $\mathbf{F}_l^{v-cd}=-\Sigma_{\mathbf{R}}\nabla_l U^{v-cd}(\mathbf{r}_l-\mathbf{R})$ is the force of interaction with the CDL, $\mathbf{R}$ denotes the CDL positions, $\mathbf{F}_d$ is the driving force, and $\mathbf{\Gamma}_l$ is the random force appropriate for temperature T.

In the absence of driving ($\mathbf{F}_d=0$), the equilibrium phases of this system (hereafter called zero-drive state) are studied (at low T) in Refs. 8–10.

For $\mathbf{F}_d\neq 0$ the simplest situation occurs at very high drives.[11] In this case the vortices center of mass (CM) move with velocity $\mathbf{V}_d=\mathbf{F}_d/\eta$ and in the CM frame of reference, defined by $\mathbf{r}_l'=\mathbf{r}_l-\mathbf{V}_d t$, the equations of motion are as in Eq. (1), but without the driving term $\mathbf{F}_d$ and with the vortex-CDL force replaced by the time-dependent interaction $\mathbf{F'}_l^{(v-cd)}(t)=\Sigma_{\mathbf{Q}}(-i\mathbf{Q})U^{v-cd}(\mathbf{Q})e^{i\mathbf{Q}\cdot\mathbf{r}_l'}e^{i\mathbf{Q}\cdot\mathbf{V}_d t}$, where $\mathbf{Q}$ denotes the CDL reciprocal lattice vectors and $U^{v-cd}(\mathbf{Q})$ is the Fourier transform of $U^{v-cd}(\mathbf{r})$. For high enough drives the Fourier components in $\mathbf{F'}_l^{(v-cd)}(t)$ for which $\mathbf{Q}\cdot\mathbf{V}_d\neq 0$ oscillate fast, thus having a negligible effect on the vortex trajectory.[11] The vortex-CDL force in the CM frame reduces then to the static one obtained by summing the Fourier components in $\mathbf{F'}_l^{(v-cd)}(t)$ with $\mathbf{Q}\cdot\mathbf{V}_d=0$ (or $\mathbf{Q}\perp\mathbf{V}_d$). This force is just that resulting from the potential obtained by averaging $U^{v-cd}(\mathbf{r})$ in the direction of drive. Thermal fluctuations lead, after sufficient time, to relaxation into the thermodynamic equilibrium state of the N_v vortices interacting between themselves and with this average potential. This state is referred to here as the infinite-drive state.

Since at low T the infinite-drive and the zero-drive states are generally different, reordering of the vortices must take place as the driving force is varied. This predicts the existence of at least two dynamical phases and, possibly, of one dynamical phase transition. One result obtained in this paper is to show that this prediction is correct. Studies of vortices interacting with a CDL carried out at $T=0$ find a rich variety of phases, but no reordering to the infinite drive state.[4,5]

For driven vortices interacting with a random pinning potential, the existence of reordering and of a dynamical transition as the driving force is varied are well established.[12] In this case the pinning potential averaged in the direction of drive remains random in the direction perpendicular to it, and has nontrivial effects on the dynamical phase diagram, as extensively discussed in Ref. 13. For motion on a periodic pinning potential, numerical simulations reported in Ref. 14 show that vortex reordering to the infinite-drive state only occurs if sufficient thermal fluctuations are present. Otherwise the vortices are trapped in a metastable state.

The numerical simulations reported here investigate the properties of the moving vortices steady states as a function of the driving force, for a range of T beginning at a value well below the infinite-drive state melting temperature, T_m, and extending up to T_m. The simulations are initialized with the vortices in the infinite-drive state and large enough F_d. In subsequent runs, at the same T, F_d is progressively decreased. The main conclusions reached by this approach are that for $T<T_m$ a dynamical phase with the spatial symmetry of the infinite-drive state, elastic flow and long-range time order exists for $F_d>F_c(T)$. At $F_d=F_c(T)$ a transition separates it from another dynamical phase with distinct spatial order and plastic flow. It is found that the transition is sharp at low T and that $F_c(T)$ increases as $T\rightarrow T_m$.

The details of the model are as follows.[14] Vortices and CD are placed on a square lattice subjected to periodic boundary conditions (hereafter called the space lattice), with

N square primitive cell of dimensions $d\times d$, oriented with the sides in the x and y directions. The vortex has a core of linear dimension $d_v > d[d_v \sim 2\xi(0)]$. The interactions between vortices and between vortices and CD are chosen to model films in the London limit. The vortex-vortex interaction potential is a screened Coulomb one,[15] appropriate for the space lattice, with a short distance cutoff to account for the vortex core.[7] That is, $U^{vv}(\mathbf{r})$ is the lattice Fourier transform of $U^{vv}(\mathbf{k}) = 4\pi^2 J \exp(-\kappa^2/\kappa_c^2)/(\kappa^2+\Lambda^{-2})$, where $J = (\phi_0^2 d_v/32\pi^2\lambda^2)$ is the energy scale for vortex-vortex interactions,[15] λ is the penetration depth, $\kappa^2 = 4\sin^2(k_x d/2) + 4\sin^2(k_y d/2)$, $\kappa_c = 2\sin(\pi d/2d_v)$ is the cutoff in k space, and Λ is the screening length ($\Lambda > \lambda$). The CD-lattice has N_{cd} sites arranged on a square lattice, with lattice constant a_{cd}, and is commensurate with the space lattice. The vortex-CD potential is chosen with depth $U^{v-cd}(0)$, range $R_{cd} > d_v$ and a spatial dependence that gives square equipotentials and an attractive pinning force of constant modulus $F_p = |U^{v-cd}(0)|/R_{cd}$. That is, $U^{v-cd}(\mathbf{r}) = U^{v-cd}(0)(1 - |x|/R_{cd})$ for $|x| \leq R_{cd}$, $-|x| \leq y \leq |x|$, and $U^{v-cd}(\mathbf{r}) = U^{v-cd}(0)(1-|y|/R_{cd})$ for $|y| \leq R_{cd}$, $-|y| \leq x \leq |y|$.

The algorithm for the simulation of this model follows the usual procedure.[16] In the results reported next space lattices with $N = 256\times 256$ and 512×512 sites are used to accommodate a CDL with $N_{cd} = 64$ and 256, respectively, both with $a_{cd} = 32d$. Other parameters are fixed at $d_v = 4d$, $\Lambda = 160d$, $U^{v-cd}(0) = -J$, $R_{cd} = 3d_v = 12d$, from which it follows that $F_p = J/12d$. The vortex systems studied have $N_v = 1.25N_{cd}$ and $2N_{cd}$ or, in terms of the magnetic induction, $B = 1.25B_\phi$ and $B = 2B_\phi$, where $B_\phi = \phi_0/a_{cd}^2$ is the matching field. Typical run times are $2-5\times 10^6$ steps of $10^{-2}\tau$ ($\tau = \eta d^2/J$ is the unit of time), after the steady state is reached. The reported results represent the average over several different realizations of the random force (~ 10). The driving force is assumed to be along y [CDL (0,1)-direction].

To characterize the dynamical phases the following quantities are calculated in the steady-state regime: (i) Time average of the individual vortex velocities, $\mathbf{v}_j$ ($j = 1, \ldots, N_v$), their mean or the center of mass (CM) velocity, $\mathbf{V}^{cm} = \Sigma_j \mathbf{v}_j/N_v$, and root-mean square deviation $\Delta V_\alpha^{cm} = \sqrt{\Sigma_j (v_{j\alpha} - V_\alpha^{cm})^2/N_v}$, where $\alpha = x,y$. (ii) Time-averaged density-density correlation function, $P(\mathbf{r})$, and its Fourier transform, the structure function, $S(\mathbf{k})$. (iii) Time-dependent correlation functions for the CM velocity, $C_\alpha^{cm}(t) = \langle V_\alpha^{cm}(t+s) V_\alpha^{cm}(s)\rangle_s$, and for the vortex velocity autocorrelation function averaged over all vortices, $C_\alpha^{sf}(t) = (1/N_v)\Sigma_i \langle v_{i\alpha}(t+s) v_{i\alpha}(s)\rangle_s$, where $\langle\ \rangle_s$ denotes average with respect to time s, and the respective Fourier transforms $C_\alpha^{cm}(\omega)$ and $C_\alpha^{sf}(\omega)$. Physically, $P(\mathbf{r})$ is proportional to the probability of finding a pair of vortices separated by $\mathbf{r}$, whereas $C_\alpha^{cm}(\omega)$ is proportional to the noise power spectrum.

The possible infinite-drive states and the corresponding T_m are determined by equilibrium Monte Carlo simulations of the model described above, with the vortex-CDL interaction potential replaced by its average in the y direction. This is a periodic washboard potential, consisting of grooves of width $2R_{cd}$ running along the y direction and separated by a_{cd} along the x direction. Inside the groove the vortex is attracted to its center by a force of constant modulus F

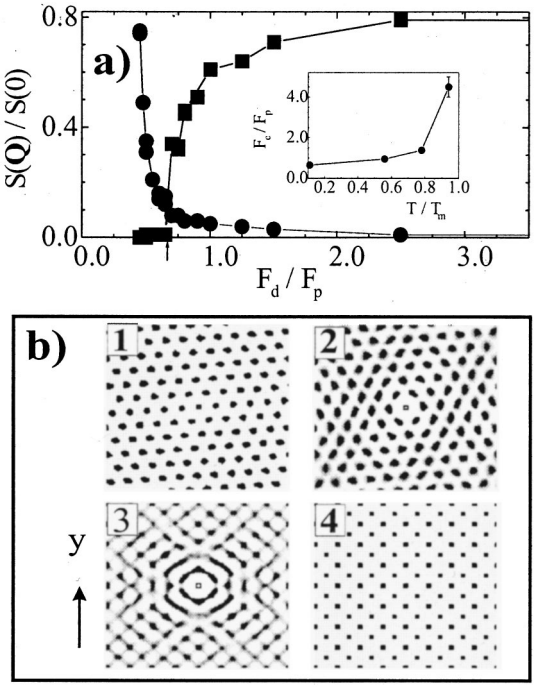

FIG. 1. (a) Structure function for $B = 2B_\phi$ and $T/T_m = 0.1$. Squares (circles): $\mathbf{k}$= typical infinite (zero)- drive state reciprocal-lattice vector of smallest modulus. Inset, F_c vs T. (b) Corresponding $P(\mathbf{r})$ for: (1) infinite-drive state, (2) elastic flow phase at $F_d = 0.7F_p$, (3) plastic flow phase at $F_d = 0.6F_p$, and (4) zero-drive state for $F_d < 0.45F_p$. The origin $\mathbf{r} = 0$ is at each picture center. Gray scale in each picture is proportional to $P(\mathbf{r})$, but scales in different pictures are unrelated.

$< F_p$ in the x direction. For $B > B_\phi$ these states have only two possible spatial orders: incommensurate (essentially triangular) at B sufficiently large, and commensurate with the x-direction periodicity at lower B. The precise B value at which the ground-state changes from one type to the other depends on a nontrivial way on the model parameters. It is found that, for the above described model parameters, two typical such infinite-drive states are the vortex lattices (VL) for $B = 2B_\phi$, with the $P(\mathbf{r})$ shown in Fig. 1(b.1), and for $B = 1.25B_\phi$ with the vortex arrangement shown in Fig. 2(a). The latter can also be seen as consisting of pairs of vortex chains located within the grooves and displaced relative to one another by half intrachain spacing. It is found that the

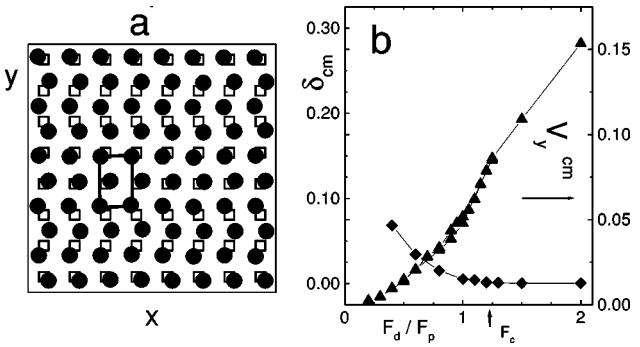

FIG. 2. $B = 1.25B_\phi$: (a) Full circles: vortex positions for infinite-drive state. Full line: VL primitive unit cell. Open squares: CDL. (b) CM velocity V_y^{cm} (units d/τ) and $\delta_{cm} = \Delta V_y^{cm}/V_y^{cm}$.

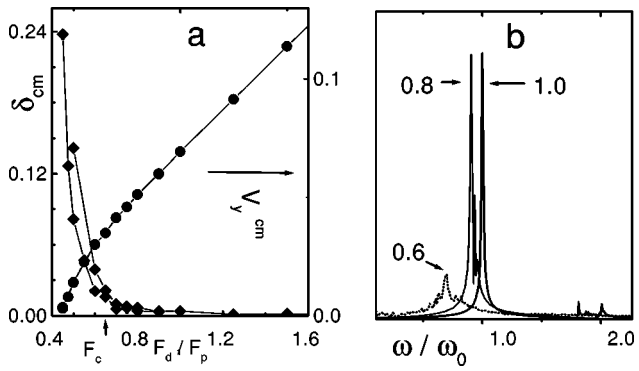

FIG. 3. $B=2B_\phi$: (a) CM velocity V_y^{cm} (units d/τ) and $\delta_{cm}=\Delta V_y^{cm}/V_y^{cm}$. (b) Correlation function $C_y^{sf}(\omega)$ at F_d/F_p values indicated in the figure. The ordinate axis (arbitrary units) in each curve is scaled to show all curves in the same graph. ω_0 denotes ω_{cm} at $F_d/F_p=1.0$. Peaks are centered at ω_{cm} in all curves.

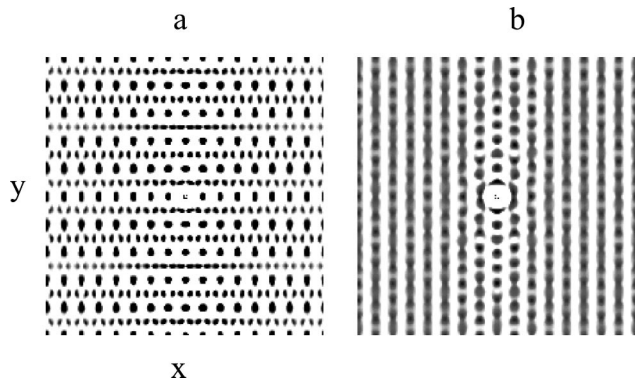

FIG. 4. $P(\mathbf{r})$ for $B=1.25B_\phi$ in 512×512 space lattice: (a) elastic flow phase at $F_d=1.3F_p$, (b) plastic flow phase at $F_d=1.2F_p$.

VL for $B=2B_\phi$ melts to a vortex liquid at $T_m=0.9J$, and that the VL for $B=1.25B_\phi$ first melts to a smectic phase at $T/T_{sm}\sim0.85J$ and then to a liquid at much higher T. The results reported here for $B=1.25B_\phi$ are restricted to $T/T_{sm}\sim0.1$. Monte Carlo simulations are also used to determine the zero-drive states for these B values. For $B=2B_\phi$ a VL commensurate with the CDL and having one extra vortex at the center of the CDL primitive unit cell is obtained, in agreement with previous results.[9,10] This state's $P(\mathbf{r})$ is shown in Fig. 1(b.4). For $B=1.25B_\phi$ a complex commensurate VL with several vortices in the unit cell is found.

The results of the dynamical simulations carried out here, to be discussed in detail next, identify two dynamical phases, elastic flow and plastic flow, and a transition between them around $F_d=F_c(T)$. It is found that for $B/B_\phi=1.25$ and $T/T_m\sim0.2$, $F_c/F_p\sim1.25$ and that for $B/B_\phi=2$ the $F_c(T)$ curve is that shown in Fig. 1(a). In both flow regimes the time-averaged velocity of all vortices is in the direction of drive. The $V_y^{cm}(F_d)$ curves (V-I curve) at low T are depicted in Figs. 2(b) and 3(a). The detailed properties of these phases are as follows.

(i) *Elastic flow*: $F_d>F_c$, *low T, both B.* The moving vortices remain localized with respect to each other around the infinite-drive state relative equilibrium positions. This is suggested by $P(\mathbf{r})$ shown in Figs. 1(b.1), 1(b.2), and 4(a). These consist of isolated spots with the symmetry of this state. As $F_d\to F_c$ these spots become larger, indicating increase in relative vortex motion in the CM frame. The time-averaged velocity of all vortices is, within the simulation errors, V_y^{cm}, since $\Delta V_\alpha^{cm}/V_y^{cm}(\alpha=x,y)$ is small for $F_d>F_c$ [Figs. 2(b), and 3(a)]. Similar results are found for $\Delta V_x^{cm}/V_y^{cm}$. Vortex motion consists of a translation in the direction of drive with V_y^{cm} and of periodic oscillations with frequency $\omega_{cm}=2\pi V_y^{cm}/a_{cd}$ and higher harmonics around the infinite-drive state equilibrium positions. These oscillations are suggested by $C_\alpha^{cm}(\omega)$ and $C_\alpha^{sf}(\omega)$ which are found to have sharp peaks at ω_{cm} and peaks with smaller amplitudes at some harmonics as illustrated in Fig. 3(b). This frequency coincides with the oscillation frequency of the vortex-CDL interaction in the frame moving with the CM. This suggests that the periodic vortex motion is the (nonlinear) elastic response of the VL to this interaction. The frequency dependence of $C_\alpha^{cm}(\omega)$ and $C_\alpha^{sf}(\omega)$ suggest long-range time order.

(ii) *Transition region*: $F_d\sim F_c$, *low T, both B.* Vortex spatial order changes in a small F_d interval. This is seen both in $P(\mathbf{r})$ and in $S(\mathbf{k})$, for $\mathbf{k}$ equal to high-drive ground-state reciprocal lattice vectors, (Fig. 1). The value of F_c is estimated as the midpoint of this interval, as indicated in Fig. 1. This rapid change in the vortex spatial order suggests a discontinuous jump in $S(\mathbf{k})$. However, the present data cannot rule out a sharp crossover. In the same F_d interval, the $V_y^{cm}\times F_d$ curves changes slope, as seen in [Figs. 2(b) and 3(a)] and the sharp peaks in $C_\alpha^{cm}(\omega)$ and $C_\alpha^{sf}(\omega)$ are found to disappear.

(iii) *Plastic flow*: $F_d<F_c$, *low T*, $B=2B_\phi$. Plastic flow sets in for F_d just below F_c and relative motion increases as F_d decreases, as evidenced by the sharp change in slope and continuous growth in $\Delta V_y^{cm}/V_y^{cm}$ shown in Fig. 3(a). The vortices become pinned in the zero-drive state for $F_d<0.45F_p$. It is found that all vortices become pinned simultaneously at $F_d=0.45F_p$. The vortices are disordered for F_d just below F_c [Fig. 1(b.3)] and, as F_d further decreases, the vortices show increasing order in the zero-drive state symmetry, as suggested by the $S(\mathbf{k})$ vs F_d curves for $\mathbf{k}$ equal to zero-drive state reciprocal lattice vectors [Fig. 1(a)]. This increase in order arises because as F_d decreases the vortices spend more of their travel time near the zero-drive state equilibrium positions. There is no long-range time order as shown by the absence of sharp peaks in the frequency dependence of $C_\alpha^{cm}(\omega)$ and $C_\alpha^{sf}(\omega)$ [Fig. 3(b)].

(iv) *Plastic flow: low T*, $F_d<F_c$, $B=1.25B_\phi$. For F_d just below F_c some spatial order remains. For $x=0$ and $x=a_{cd}$, $P(\mathbf{r})$ [Fig. 4(b)] consists of isolated spots, indicating that the double vortex chain-structure of the infinite-drive state transforms to a single chain one with, roughly, nearest-neighbor chains displaced relative to each other by half intrachain spacing, and that the vortices oscillate around the corresponding equilibrium positions. For larger x the spots become interconnected by stripes in the direction of motion, indicating that interchain relative motion at these separations, and thus plastic flow, is taking place. The behavior of $\Delta V_y^{cm}/V_y^{cm}$ across the transition [Fig. 2(b)] shows little change, suggesting that plastic flow is weak. The frequency dependence of $C_\alpha^{cm}(\omega)$ and $C_\alpha^{sf}(\omega)$ is found to remain

sharply peaked. These results are interpreted as indicating that vortices move together with the chain, oscillating around their equilibrium position within it, but relative motion between chains is taking place. As F_d decreases further plastic flow continues with increasing $\Delta V_y^{cm}/V_y^{cm}$, but the vortices remain ordered in single chains and are unpinned for $F_d > 0$ [Fig. 2(b)]. It is expected that vortex reordering and pinning would take place as F_d decreases. The failure to see this in the present simulations is interpreted as evidence that trapping in a metastable state is taking place.

(v) *T dependence*. As T increases $F_c(T)$ also increases, because thermal fluctuations make the infinite-drive state VL softer. Thermal fluctuations also lead to smaller values of $S(\mathbf{k})$. This makes the dynamical transitions described above more difficult to observe, particularly for $B = 1.25B_\phi$. For $B = 2B_\phi$ the $F_c(T)$ curve is shown in Fig. 1(a).

For other values of $B > B_\phi$, and drive in the (0,1) or (1,0) directions, the possible infinite-drive states are either a nearly triangular VL, or a VL with n vortex chains trapped in each groove, so that a similar dynamical phase diagram is anticipated.

The experimental verification of the dynamical phases and of the transition predicted in this paper may be possible in clean superconducting films with sufficient thermal fluctuations to allow relaxation to the infinite-drive state to take place at large drives. Signatures of these phases are present in the V-I curve and in the noise power spectrum. Visualization of the spatial order may also be possible using decoration or fast scanning tunnel microscope techniques.

*Email address: gmc@if.ufrj.br

[1] A. N. Lykov, Adv. Phys. **42**, 263 (1993).

[2] V. V. Metlushko *et al.*, Solid State Commun. **91**, 331 (1994); M. Baert *et al.*, Phys. Rev. Lett. **74**, 3269 (1995); E. Rosseel *et al.*, Phys. Rev. B **53**, R2983 (1996); V. V. Moshchalkov *et al.*, *ibid.* **54**, 7385 (1996); K. Harada *et al.*, Science **274**, 1167 (1996); J.-Y. Lin *et al.*, Phys. Rev. B **54**, R12 717 (1996); L. Van Look *et al.*, *ibid.* **60**, 6998 (1999).

[3] P. Martinoli, Phys. Rev. B **17**, 1175 (1978).

[4] C. Reichhardt *et al.*, Phys. Rev. B **54**, 16 108 (1996); **57**, 7937 (1998); **58**, 6534 (1998); Phys. Rev. Lett. **78**, 2648 (1997).

[5] C. Reichhardt and F. Nori, Phys. Rev. Lett. **82**, 414 (1999).

[6] V. I. Marconi and D. Dominguez, Phys. Rev. Lett. **82**, 4922 (1999).

[7] E. H. Brandt, Rep. Prog. Phys. **58**, 1465 (1995).

[8] M. G. Blamire, J. Low Temp. Phys. **68**, 335 (1987).

[9] C. Reichhardt *et al.*, Phys. Rev. B **57**, 7937 (1998).

[10] W. A. M. Morgado and G. Carneiro, Physica C **328**, 195 (1999).

[11] A. Schmid and W. Hauger, J. Low Temp. Phys. **11**, 667 (1973); A. E. Koshelev and V. M. Vinokur, Phys. Rev. Lett. **73**, 3580 (1994).

[12] S. Bhattacharya and M. J. Higgins, Phys. Rev. Lett. **70**, 2617 (1993); U. Yaron *et al.*, *ibid.* **73**, 2748 (1994); Nature (London) **376**, 753 (1995); A. Duarte *et al.*, Phys. Rev. B **53**, 11 336 (1996); F. Pardo *et al.*, Phys. Rev. Lett. **78**, 4633 (1997); M. Marchevsky *et al.*, *ibid.* **78**, 531 (1997).

[13] T. Giamarchi and P. Le Doussal, Phys. Rev. Lett. **76**, 3408 (1996); Physica C **282**, 363 (1997); P. LeDoussal and T. Giamarchi, Phys. Rev. B **57**, 11 356 (1998).

[14] G. Carneiro, J. Low Temp. Phys. **117**, 1323 (1999).

[15] P. Minnhagen, Rev. Mod. Phys. **59**, 1001 (1987).

[16] D. W. Heermann, *Computer Simulation Methods in Theoretical Physics* (Springer, Berlin, 1990), Chap. 4.